Article

Role for Bound Water and CH–π Aromatic Interactions in Photosynthetic Electron Transfer

Colette A. Sacksteder, Shana L. Bender, and Bridgette A. Barry

J. Am. Chem. Soc., **2005**, 127 (21), 7879-7890• DOI: 10.1021/ja050659a • Publication Date (Web): 10 May 2005

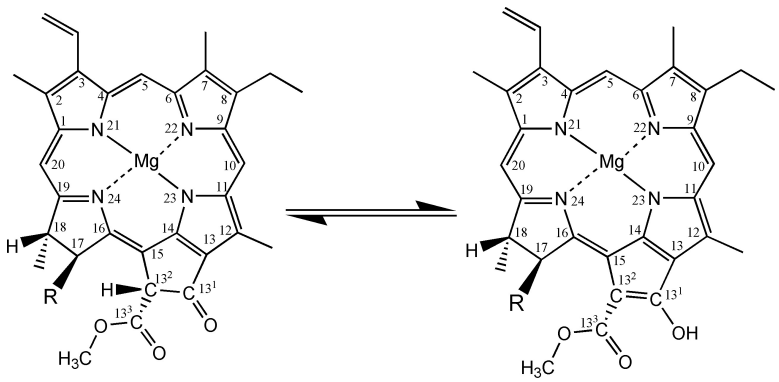

More About This Article

Additional resources and features associated with this article are available within the HTML version:

- Supporting Information
- Links to the 2 articles that cite this article, as of the time of this article download
- Access to high resolution figures
- Links to articles and content related to this article
- Copyright permission to reproduce figures and/or text from this article

View the Full Text HTML

J|A|C|S
ARTICLES
Published on Web 05/10/2005

Role for Bound Water and CH−π Aromatic Interactions in Photosynthetic Electron Transfer

Colette A. Sacksteder,[‡] Shana L. Bender,[†] and Bridgette A. Barry*,[†]

Contribution from the Department of Biochemistry, Molecular Biology, and Biophysics, University of Minnesota, St. Paul, Minnesota 55108

Received February 1, 2005; E-mail: bridgette.barry@chemistry.gatech.edu

Abstract: Photosystem I (PSI) is one of two photosynthetic reaction centers present in plants, algae, and cyanobacteria and catalyzes the reduction of ferredoxin and the oxidation of cytochrome *c* or plastocyanin. The PSI primary chlorophyll donor, which is oxidized in the primary electron-transfer events, is a heterodimer of chl *a* and *a*′ called P_{700}. It has been suggested that protein relaxation accompanies light-induced electron transfer in this reaction center (Dashdorj, N.; Xu, W.; Martinsson, P.; Chitnis, P. R.; Savikhin, S. *Biophys. J.* **2004**, *86*, 3121. Kim, S.; Sacksteder, C. A.; Bixby, K. A.; Barry, B. A. *Biochemistry* **2001**, *40*, 15384). To investigate the details of electron transfer and relaxation events in PSI, we have employed several experimental approaches. First, we report a pH-dependent viscosity effect on P_{700}^+ reduction; this result suggests a role for proton transfer in the PSI electron-transfer reactions. Second, we find that changes in hydration alter the rate of P_{700}^+ reduction and the interactions of P_{700} with the protein environment. This result suggests a role for bound water in electron transfer to P_{700}^+. Third, we present evidence that deuteration of the tyrosine aromatic side chain perturbs the vibrational spectrum, associated with P_{700}^+ reduction. We attribute this result to a linkage between CH−π interactions and electron transfer to P_{700}^+.

Photosystem I (PSI)[1] is a multisubunit membrane protein essential for photosynthesis in plants, algae, and cyanobacteria. As one of two light-activated reaction centers located in the thylakoid membrane, PSI is responsible for the transfer of electrons from one of the mobile electron carriers, plastocyanin or cytochrome c_6, to the electron acceptor, ferredoxin. Cyanobacterial PSI consists of 12 subunits,[2,3] 3 of which, PsaA, PsaB, and PsaC, bind electron-transfer cofactors. PsaA and PsaB subunits form the transmembrane heterodimeric PSI core, and PsaC is an extrinsic, stromal subunit. Electron transfer in PSI initiates with photoexcitation of the primary donor, P_{700}, which is a chlorophyll (chl) *a*/*a*′ heterodimer (Figure 1A). Chl *a*′ is the result of epimerization of chl *a* at carbon 13[2] (Figure 1A). The primary donor is flanked by two additional accessory chlorophylls.[2,3]

In this paper, the terms P_A and P_B will be used to refer to the chl *a*′ and chl *a* components of P_{700}, respectively (Figure 1B). P_A is ligated by a histidine side chain in the PsaA subunit; P_B is ligated by a histidine side chain in the PsaB subunit.[2,3] The electron acceptor molecules, which are sequentially reduced in PSI after P_{700} photoexcitation, are chl A_0, phylloquinone A_1, and three iron sulfur clusters, F_X, F_A, and F_B.[4] The electron-accepting cofactors, A_0 and A_1, are arranged with apparent C_2 structural symmetry around P_{700}. This C_2 symmetry is broken by hydrogen-bonding interactions between amino acid residues and P_A (Figure 1B). The keto carbonyl group (Figure 1A) of P_A forms a hydrogen bond with Thr A743,[5] which is, in turn, within hydrogen-bonding distance of water (Figure 1B). This water molecule (W19) is central to the hydrogen-bonding network because it is also within hydrogen-bonding distance from Ser A607 and Tyr A603. Hydrogen-bonding interactions between P_A and another tyrosine side chain (A735) (Figure 1B) are also possible.[2,3] While this network of hydrogen bonding distinguishes P_A and P_B, it has been suggested that electron transfer in PSI may be bidirectional and may involve reduction of both electron-transfer pathways with different rates (refs 6 and 7 but see ref 8).

Water−protein interactions are known to play an important role in a variety of protein processes, such as enzyme catalysis, protein folding, dynamics, and conformational stability (for review, see ref 9). This is evident in photosynthetic proteins. An example is the bacteriorhodopsin family of proton pumps, in which water is a critical component of the hydrogen-bonded

[†] Present address: Department of Chemistry and Biochemistry and the Petit Institute for Bioengineering and Bioscience, Georgia Institute of Technology, Atlanta, GA 30332.

[‡] Present address: Department of Cell Biology and Biochemistry, Biological Sciences Division, Pacific Northwest National Laboratory, Richland, WA 99352.

(1) Golbeck, J. H. In *The Molecular Biology of Cyanobacteria*; Bryant, D. A., Ed.; Kluwer Academic Publishers: Dordrecht, The Netherlands, 1994; Vol. 1, pp 319−360.
(2) Fromme, P.; Jordan, P.; Krauss, N. *Biochim. Biophys. Acta* **2001**, *1507*, 5−31.
(3) Jordan, P.; Fromme, P.; Witt, H. T.; Klukas, O.; Saenger, W.; Krauss, N. *Nature* **2001**, *11*, 909−917.
(4) Brettel, K. *Biochim. Biophys. Acta* **1997**, *1318*, 322−373.
(5) Witt, H.; Schlodder, E.; Teutloff, C.; Niklas, J.; Bordignon, E.; Carbonera, D.; Kohler, S.; Labahn, A.; Lubitz, W. *Biochemistry* **2002**, *41*, 8557−8569.
(6) Ramesh, V. M.; Gibasiewicz, K.; Lin, S.; Bingham, S. E.; Webber, A. N. *Biochemistry* **2004**, *43*, 1369−1375.
(7) Guergova-Kuras, M.; Boudreaux, B.; Joliot, A.; Joliot, P.; Redding, K. *Proc. Natl. Acad. Sci. U.S.A.* **2001**, *98*, 4437−4442.
(8) Cohen, R.; Shen, G.; Golbeck, J.; Xu, W.; Chitnis, P.; Valieva, A.; van der Est, A.; Pushkar, Y.; Stehlik, D. *Biochemistry* **2004**, *43*, 4741−4754.
(9) Mattos, C. *Trends Biochem. Sci.* **2002**, *27*, 203−208.

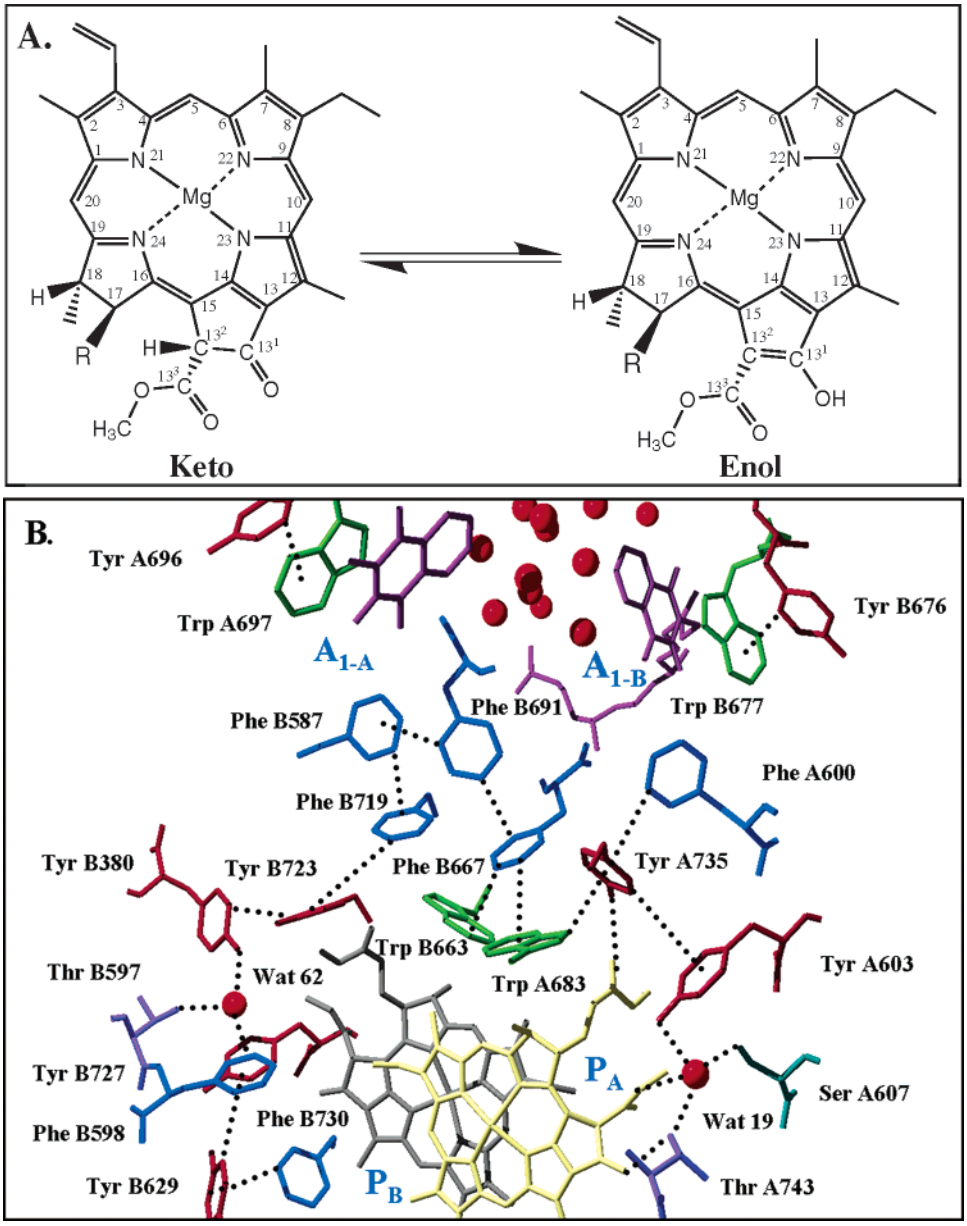

Figure 1. (A) Structure of chl *a* (left) and its enol tautomer (right). Tautomerization results in deprotonation at $C13^2$ and the formation of the 13^1 enol (right). The R group corresponds to the phytyl tail. (B) View from the 2.5 Å X-ray crystal structure of *Synechococcus elongatus* PSI (PDB file accession number 1JB0) showing possible water and aromatic interactions with electron-transfer cofactors. P_B and P_A (chl *a* and chl *a*′) are shown, as well as the A_1 phylloquinones (labeled A_{1-A}, A_{1-B}). The accessory and A_0 chl molecules are not shown. In (B), a grouping of waters and potential CH$-\pi$ interactions are shown near the A_1 cofactors. A network of potential aromatic interactions in the vicinity of P_{700} are also presented. These aromatic interactions include possible hydrogen-bonding linkages with waters 62 and 19. The figure was generated using Swiss-Pdb Viewer (v3.7; www.expasy.ch/spdbv) and rendered using POV-Ray (v3.6; www.povray.org).

water network through which proton transfer occurs.[10,11] In the reaction center of the purple bacterium, *Rhodobacter sphaeroides*, changes in water−protein structure have been reported to alter picosecond electron-transfer rates.[12] In PSII, changes in osmolyte or cosolvent concentration have been shown to alter oxygen evolution activity.[13]

It has also been suggested that water may play a role in cyanobacterial PSI electron transfer.[14,15] At this point in refinement, the locations of some, but probably not all, bound water molecules have been identified in the PSI crystal structure.[2,3] In addition to the water molecules near P_A (described above), water is bound to the central Mg in the accessory chlorophylls. There are also a number of assigned water molecules near F_X and A_1.[2,3] We previously reported the perturbation of internal or bound water molecules upon P_{700} photooxidation in PSI.[14] Recently, it was suggested that the density of water molecules near the electron-transfer cofactors A_1 and F_X may be a crucial component in protein flexibility, effective charge screening, and the facilitation of PSI electron transfer.[15]

(10) Lanyi, J. K. *Mol. Membrane Biol.* **2004**, *21*, 143−150.
(11) Furutani, Y.; Kandori, H. *Mol. Membrane Biol.* **2002**, *19*, 257−265.
(12) Paschenko, V. Z.; Gorokhov, V. V.; Grishanova, N. P.; Goryacheva, E. A.; Korvatovsky, B. N.; Knox, P. P.; Zakharova, N. I.; Rubin, A. B. *Biochim. Biophys. Acta* **1998**, *1364*, 361−372.
(13) Halverson, K. M.; Barry, B. A. *Biophys. J.* **2003**, *85*, 1317−1325.
(14) Kim, S.; Sacksteder, C. A.; Bixby, K. A.; Barry, B. A. *Biochemistry* **2001**, *40*, 15384−15395.
(15) Dashdorj, N.; Xu, W.; Martinsson, P.; Chitnis, P. R.; Savikhin, S. *Biophys. J.* **2004**, *86*, 3121−3130.

It has been proposed that P_{700} may partially enolize (Figure 1A) when it is oxidized.[14,16,17] Such an enolization reaction would involve full or partial proton transfer to the keto oxygen of P_{700} from a nearby amino acid or a water molecule (Figure 1A). There is also evidence of a strong hydrogen bond to the keto oxygen of P_{700}^+; it has been suggested that the strength of this hydrogen bond is influenced by nearby water molecules.[2,3,5,18,19] If redox-linked changes in the strength of this hydrogen bond occur, then this idea also predicts that partial proton transfer will accompany the electron transfer. The ideas of enolization and redox-linked changes in hydrogen bonding are related, with enolization necessitating a bond order change in the chlorin ring (Figure 1A). Both of these ideas suggest that internal water molecules may play a role in PSI electron transfer.

It is also noteworthy that an extensive set of aromatic interactions exists in the vicinity of the primary donor (Figure 1B), the electron-accepting chlorophyll, A_0, A_1, and F_X.[2,3] The location of aromatic side chains near P_{700} is shown in Figure 1B. In the PsaA subunit, Y735 and Y603 can potentially form a CH$-\pi$ interaction, with Y735 as the C$-$H donor and Y603 as the aromatic acceptor. Y603 may also hydrogen bond to the water molecule (W19) near P_A, and Y735 is in hydrogen-bonding distance from the ester carbonyl group of the P_A phytyl tail (Figure 1A,B). In addition, each A_1 quinone is in proximity to the indole side chain of a tryptophan, and this tryptophan may interact with a nearby conserved tyrosine. Therefore, the PSI X-ray structure suggests that interactions among aromatic amino acid side chains may play a role in PSI electron transfer.[2,3]

In this work, we used FT-IR (Fourier transform infrared) and EPR (electron paramagnetic resonance) spectroscopy to investigate the importance of bound water and aromatic interactions in electron transfer in cyanobacterial PSI. PSI reaction centers were isolated from the cyanobacterium, *Synechocystis* sp. PCC 6803. We present EPR kinetic data, which show that ^2H_2O slows the reduction rate of P_{700}^+. We attribute this decrease in rate to a pH-dependent viscosity effect. We also show that a decrease in hydration significantly impedes the reduction of P_{700}^+. In addition, we have used isotopic labeling of tyrosine to provide evidence for a perturbation of aromatic CH$-\pi$ interactions during PSI electron transfer.

Materials and Methods

Photosystem I Preparations. Trimeric cyanobacterial PSI samples from *Synechocystis* sp. PCC 6803 cultures were purified as previously described (see ref 14 and references therein). Cultures, in which tyrosine was $^2H_4$ ring-labeled (L-tyrosine-ring-d4 D-98%, Cambridge Isotope Laboratories, Andover, MA), were obtained using feedback inhibition of the shikimate pathway.[20] After purification, samples were dialyzed against 5 mM HEPES/NaOH, pH 7.5, and concentrated using a Centricon YM-100 filter (Amicon, Beverly, MA) either to 2.0 or 1.2 mg chl/mL for wild type and labeled samples, respectively. The steady-state oxygen consumption rates of the PSI samples[14] were in the range from 100 to 140 μmol O_2 (mg chl/h)$^{-1}$.

Solvent Exchange. Buffers for viscosity experiments contained 5 mM HEPES/NaOH and 0.05% dodecyl maltoside (Anatrace, Maumee, OH). The H_2O and ^2H_2O buffers were adjusted to the appropriate pH or p^{2}H of 7.0, 7.5, or 8.0 using NaOH or NaO^{2}H (99.9% ^{2}H label, Cambridge Isotope Laboratories, Inc, Andover, MA). The p^{2}H is reported as the uncorrected meter reading from the pH electrode. This method has been previously suggested because ^{2}H effects on the glass electrode and on the pK_a values of most acid and bases are compensating.[21] The solvent exchange was performed using Centricon YM-100 filters (Amicon, Beverly, MA). Three dilution/concentration steps were performed, followed by a final dilution. Dilutions ranged from approximately 7 to 35-fold. Samples were then incubated for 3 h at 6 °C in the exchange buffer and frozen and thawed prior to experimental procedures.[14] Final concentrations were 2.0 mg chl/mL.

The viscosity of ^2H_2O is 1.2 times the viscosity of ^1H_2O.[22] To mimic the viscosity change in ^2H_2O,[23−25] experiments were also conducted in a buffer, containing 5 mM HEPES/NaOH, pH 8.0, 0.05% dodecyl maltoside, and either 9% glycerol (w/w) or 8% sucrose (w/w). These buffers have the same viscosity as 100% ^2H_2O (CRC Handbook of Chemistry).

EPR Spectroscopy and Viscosity Effects. EPR spectra were acquired at room temperature using aqueous PSI samples in a quartz EPR flat cell (Wilmad, Buena, NJ). Data were collected on a Bruker EMX 6/1 spectrometer equipped with a Bruker ST-TE cavity. Potassium ferrocyanide stocks were made in the appropriate buffer just prior to each experiment and were added to the sample to give a final concentration of 3 mM. The decay kinetics of P_{700}^+, following an actinic flash, were monitored at a constant magnetic field as a function of time. The actinic flash was provided by the frequency-doubled, 532 nm output of a Surelite Nd:YAG laser (Continuum, Santa Clara, CA), with an average pulse energy of 45 mJ. The laser spot was expanded with a cylindrical lens to an approximate size of 5 × 25 mm. PSI samples were illuminated in the EPR cavity. The magnetic field selected was the positive peak of the field-swept P_{700}^+ EPR spectrum (Figure 2A, asterisk), which was generated under constant illumination with a red- and heat-filtered fiber optic illuminator (Dolan Jenner, Woburn, MA). Three sets of data were collected and averaged on each sample; data from three different samples were obtained for each condition. The field-swept spectrum was recorded in the dark prior to each data set to verify that complete decay of P_{700}^+ had occurred during dark adaptation. The amplitudes of these field-swept spectra were compared before and after each data set to ensure that repeated actinic laser flashes did not degrade the sample. The amplitude of the signal acquired immediately after the actinic flash was the same on every flash. To obtain the rate constants, kinetic data were fit to a single exponential decay using IGOR PRO software (Lake Oswego, OR). Spectral conditions for field-swept spectra were: microwave frequency, 9.75 GHz; microwave power, 20 mW; modulation amplitude, 2.0 G; scan time, 41.9 s; receiver gain, 2.8 × 10^4; and time constant, 655.4 ms. To measure the decay kinetics, conditions were the same as above with the following exceptions: scan time, 1342 s; time constant, 81.9 ms.

EPR Spectroscopy and Hydration Effects. EPR data were obtained as above with the following exceptions. Each sample contained 200 μg of chlorophyll and 3 mM potassium ferrocyanide and was distributed across five acetate strips. Samples were then concentrated either for 2 min (hydrated) or 10−15 min (partially dehydrated) with a flow of nitrogen gas. The sample strips were stacked and inserted into a quartz EPR tube, and data were obtained at −10 °C. The EPR spectrometer was equipped with a variable-temperature Wilmad dewar, and the temperature was maintained with a stream of cold nitrogen flowing through a dry ice ethanol bath.[26] Spectral conditions were: constant

(16) Wasielewski, M.; Norris, J.; Shipman, L.; Lin, C.; Svec, W. *Proc. Natl. Acad. Sci. U.S.A.* **1981**, *78*, 2957−2961.
(17) Käss, H.; Fromme, P.; Witt, H. T.; Lubitz, W. *J. Phys. Chem. B* **2001**, *105*, 1225−1239.
(18) Breton, J.; Nabedryk, E.; Leibl, W. *Biochemistry* **1999**, *38*, 11585−11592.
(19) Pantelidou, M.; Chitnis, P.; Breton, J. *Biochemistry* **2004**, *43*, 8380−8390.
(20) Barry, B. A.; Babcock, G. T. *Proc. Natl. Acad. Sci. U.S.A.* **1987**, *84*, 7099−7103.
(21) Schowen, K. B.; Schowen, R. L. *Methods Enzymol.* **1982**, *87*, 551−606.
(22) Baker, W. E. *J. Chem. Phys.* **1936**, *4*, 294−295.
(23) Glickman, M. H.; Klinman, J. P. *Biochemistry* **1995**, *34*, 14077−14092.
(24) Karsten, W. E.; Lai, C.-J.; Cook, P. F. *J. Am. Chem. Soc.* **1995**, *117*, 5914−5918.
(25) Itzhaki, L. S.; Evans, P. A. *Protein Sci.* **1996**, *5*, 140−146.
(26) Kim, S.; Ayala, I.; Steenhuis, J. J.; Gonzalez, E. T.; Razeghifard, M. R.; Barry, B. A. *Biochim. Biophys. Acta* **1998**, *1366*, 330−354.

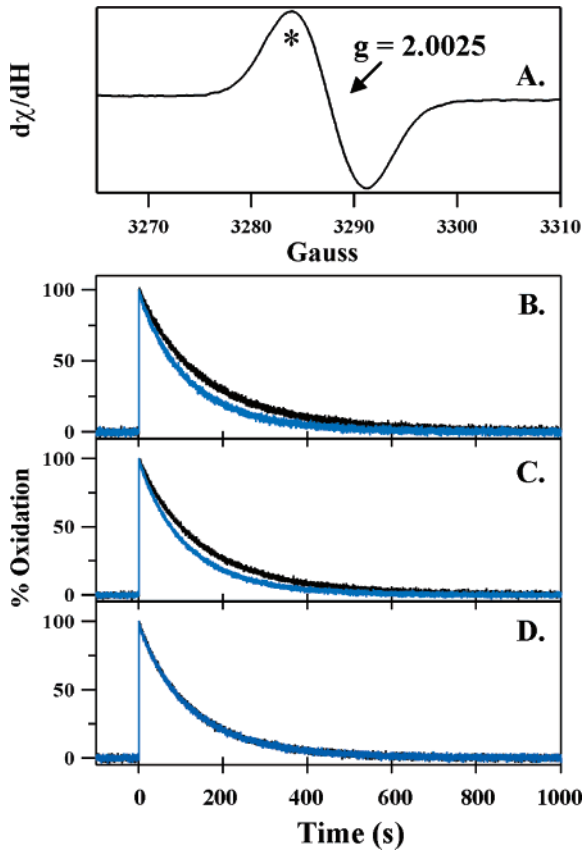

Figure 2. ^2H_2O effects on P_{700} reduction kinetics, as measured by EPR spectroscopy at room temperature. In (A), the field-swept EPR spectrum of P_{700}^+ is presented. The asterisk denotes the field position at which EPR kinetic data (B−D) were acquired. In (B−D), the kinetics of P_{700}^+ reduction by 3 mM potassium ferrocyanide were recorded after a single, 532 nm laser flash. Data were acquired in ^1H_2O (blue line) and ^2H_2O (black line) at p^1H/p^2H 8.0 (B), 7.5 (C), and 7.0 (D). Rate constants were derived from a single exponential fit to the kinetic data and are presented in Table 1. Spectral conditions are given in the Materials and Methods section.

magnetic field, 3474 G; microwave frequency, 9.21 GHz; microwave power, 4 mW; modulation amplitude, 2.0 G; receiver gain, 2.0×10^5; time constant, 81.9 ms; and scan time, 2684 s (partially dehydrated) and 168 s (hydrated). The average pulse energy was ∼160 mJ. Three data sets were averaged per sample, and two samples were used per condition.

FT-IR Spectroscopy. FT-IR spectra were collected at −10 °C as described previously.[26] Samples contained 3 mM potassium ferricyanide and 3 mM potassium ferrocyanide and were dried at room temperature under a steady flow of nitrogen gas. Drying times were 25 or 105 min for minimally and partially dehydrated samples, respectively. Because of fluctuation in the spectral background, more hydrated samples could not be used. Spectral conditions were as follows: resolution, 4 cm^{-1}; mirror velocity, 2.5 cm/s; apodization function, Happ-Genzel; level of zero filling, 2; data acquisition time, 4.0 min. Data were obtained either in the dark or under continuous illumination with red- and heat-filtered light, as previously described. A 90 min dark relaxation time was used between illuminations.[26] The data are an average of 18 spectra and were normalized for small differences in sample concentration and path length using the amplitude of the amide II band in the infrared absorption spectra. The second derivative of the amide I region (1600−1700 cm^{-1}) was calculated using Igor Pro (WaveMetrics, Inc., Lake Oswego, OR). The results were multiplied by −1 for presentation.

Results

Viscosity Effects on the P_{700}^+ Reduction Rate. The EPR spectrum of P_{700}^+ can be detected at room temperature. As expected,[27] the signal has a *g* value at 2.002 and a hyperfine splitting of 7 G (Figure 2A). The rate of P_{700}^+ reduction, after a 532 nm laser flash, was monitored by EPR transient kinetics at a fixed magnetic field (Figure 2A, asterisk and Figure 2B, blue line). At pH 7.0, the half-time ($t_{1/2}$) for P_{700}^+ reduction was measured to be 81 s (Table 1). Potassium ferrocyanide is present in the PSI samples; this reagent acts as an electron donor to P_{700}^+. Therefore, P_{700}^+ decay after a single flash could be due either to $P_{700}^+/F_{A/B}^-$ charge recombination or to P_{700}^+ reduction by potassium ferrocyanide. Half-times ($t_{1/2}$) for P_{700}^+/F_{AB}^- charge recombination are approximately 40−70 ms at room temperature.[4,28,29] In the measurements reported here, data points were recorded at 330 ms intervals. Therefore, the measured decay kinetics (Figure 2B−D) reflect the reduction of P_{700}^+ by potassium ferrocyanide rather than charge recombination. In agreement with this expectation, we found that the measured rate of P_{700}^+ decay depended linearly on the ferrocyanide concentration. For example, we found a rate stimulation of (2.16 ± 0.05)-fold when samples containing 4 and 2 mM ferrocyanide were compared (2.0 predicted), a rate stimulation of (1.61 ± 0.08)-fold when samples containing 3 and 2 mM ferrocyanide were compared (1.5 predicted), and a rate stimulation of (1.36 ± 0.07)-fold when samples containing 4 and 3 mM ferrocyanide were compared (1.3 predicted). In centers in which P_{700}^+ is reduced by ferrocyanide, $F_{A/B}^-$ must be slowly oxidized by endogenous oxidants between the actinic flashes, which occur at 15 min intervals.

The rate of P_{700}^+ reduction was monitored by EPR transient kinetics at three different p^1H/p^2H values (Figure 2B−D). The experimental data were fit with a single exponential function to derive a rate constant (Table 1). No effect on the decay rate was observed over the pH range of 7.0−8.0 in H_2O buffers (Figure 2B−D, blue lines; Table 1). In ^2H_2O buffers at p^2H 7.5 and 8.0, there was an observed decrease in the rate (Figure 2B−D, black lines; Table 1) relative to ^1H_2O. The resulting calculated ratios were 1.27 ± 0.06 (pH/p^2H 7.5) and 1.20 ± 0.10 (p^1H/p^2H 8.0) (Table 1). There was no significant difference in rate at p^1H/p^2H 7.0 (Table 1). The rate differences of 1.2-fold at

Table 1. ^2H_2O Effects on the Rate Constants of P_{700}^+ Reduction, as Measured by EPR Spectroscopy at Room Temperature[a]

p^1H/p^2H	k (^1H_2O) [10^{-3} s^{-1}]	k (^2H_2O) [10^{-3} s^{-1}]	k (^1H_2O)/k (^2H_2O)	k (^1H_2O)/k (^2H_2O)
8.0	8.40 ± 0.25	6.98 ± 0.67	1.20 ± 0.10[b]	1.20 ± 0.12[c]
7.5	8.82 ± 0.38	6.95 ± 0.25	1.27 ± 0.06	1.27 ± 0.07
7.0	8.53 ± 0.75	8.19 ± 0.64	1.04 ± 0.02	1.04 ± 0.12

[a] Experimental procedures are described in the Materials and Methods section. [b] Standard deviations and means for k (^1H_2O)/k (^2H_2O) were calculated from the ratios of ^1H_2O and ^2H_2O rate constants obtained *from the same sample*. This pairing procedure eliminates a source of nonrandom error. These ratios were then averaged over different samples to give the standard deviation shown. Comparison of the means at the 99% confidence interval reveals a significant difference in the ratios measured at p^1H/p^2H 8.0 and 7.0 and in the ratios measured at p^1H/p^2H 7.5 and 7.0 (8 degrees of freedom). [c] Standard deviations and means for k (^1H_2O)/k (^2H_2O) were calculated by propagation of the standard deviation that was determined for the individual rate constants. This procedure assumes that all sources of error are random, which is not the case in these experiments. However, comparison of the means at the 95% confidence interval still reveals a significant difference in the ratios measured at p^1H/p^2H 7.5 and 7.0 (8 degrees of freedom).

(27) Setif, P.; Mathis, P. *Arch. Biochem. Biophys.* **1980**, *294*, 477−485.
(28) Hiyama, T.; Ke, B. *Arch. Biochem. Biophys.* **1971**, *147*, 99−108.
(29) Gong, X.-M.; Agalarov, R.; Brettel, K.; Carmeli, C. *J. Biol. Chem.* **2003**, *278*, 19141−19150.

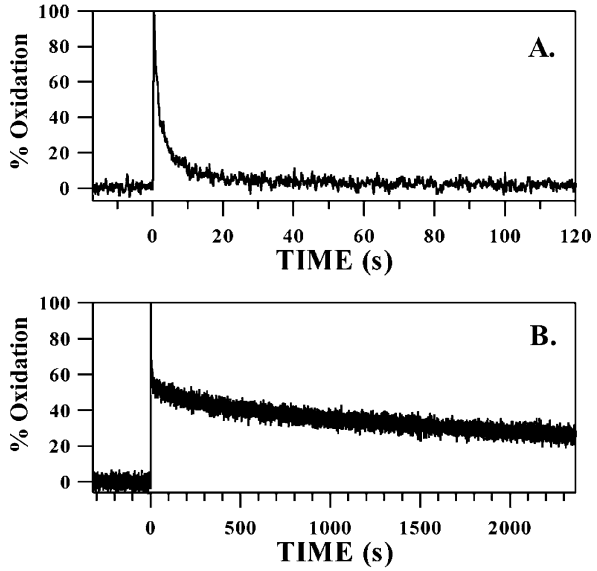

Figure 3. Dehydration effects on P_{700}^+ reduction kinetics, as measured by EPR spectroscopy at −10 °C and pH 7.5. In (A) and (B), EPR kinetic data were recorded in hydrated and partially dehydrated PSI, respectively. Derived rate constants were obtained by a single exponential fit to the data and were 0.45 ± 0.12 s^{-1} for hydrated PSI (A) and $8.9 \times 10^{-4} \pm 1.7 \times 10^{-4}$ s^{-1} for partially dehydrated PSI (B). PSI samples contained 3 mM potassium ferrocyanide and were frozen on a Mylar support. Other conditions are given in the legend for Figure 2 and in the Materials and Methods section.

p^1H/p^2H 7.5 and 8.0 correlate well with the known viscosity difference between ^1H_2O and ^2H_2O.[22] To test whether the effect of ^2H_2O at p^2H 7.5 and 8.0 was due to a viscosity or a solvent isotope effect, experiments were conducted in sucrose (8%) and glycerol (9%) solutions prepared to have the same viscosity as 100% ^2H_2O.[23−25] At pH 8.0, the ratio of rate constants measured in 9% glycerol buffer was 1.85 ± 0.13, and the ratio of rate constants measured in 8% sucrose buffer was 1.43 ± 0.13. Because 8% sucrose and 9% glycerol also decreased the rate at pH 8.0, we attribute the ^2H_2O effect to a viscosity effect on the reduction reaction. At pH 7.0, no significant glycerol effect was observed (ratio = 0.90 ± 0.06); this result shows that the viscosity effect is pH dependent.

Hydration Effects on the P_{700}^+ Reduction Rate. Figure 3 shows the effect of hydration state on the decay kinetics of P_{700}^+, as assessed by EPR spectroscopy at 263 K (−10 °C). Samples contained the electron donor, potassium ferrocyanide. A low temperature was chosen, where PSI samples are frozen, to minimize the influence of potassium ferrocyanide diffusion on the reaction rate. Figure 3A was acquired from hydrated PSI samples, and Figure 3B was acquired from partially dehydrated PSI samples. These samples were deposited on Mylar strips to mimic conditions in the FT-IR experiments. Kinetic data were fit with a single exponential decay and showed a ∼600-fold decrease in the rate of P_{700}^+ decay in the partially dehydrated sample (Figure 3B), as compared to that of the hydrated sample (Figure 3A). Derived rate constants were 0.45 ± 0.12 s^{-1} for the hydrated sample (Figure 3A) and (8.9 ± 1.7) × 10^{-4} s^{-1} for the partially dehydrated sample (Figure 3B). While $P_{700}^+/F_{A/B}^-$ charge recombination half-times have not been reported at this temperature and while charge recombination does become slower at lower temperatures,[4] a half-time of ∼230 ms can be estimated from data reported at 233 K.[30] This analysis suggests

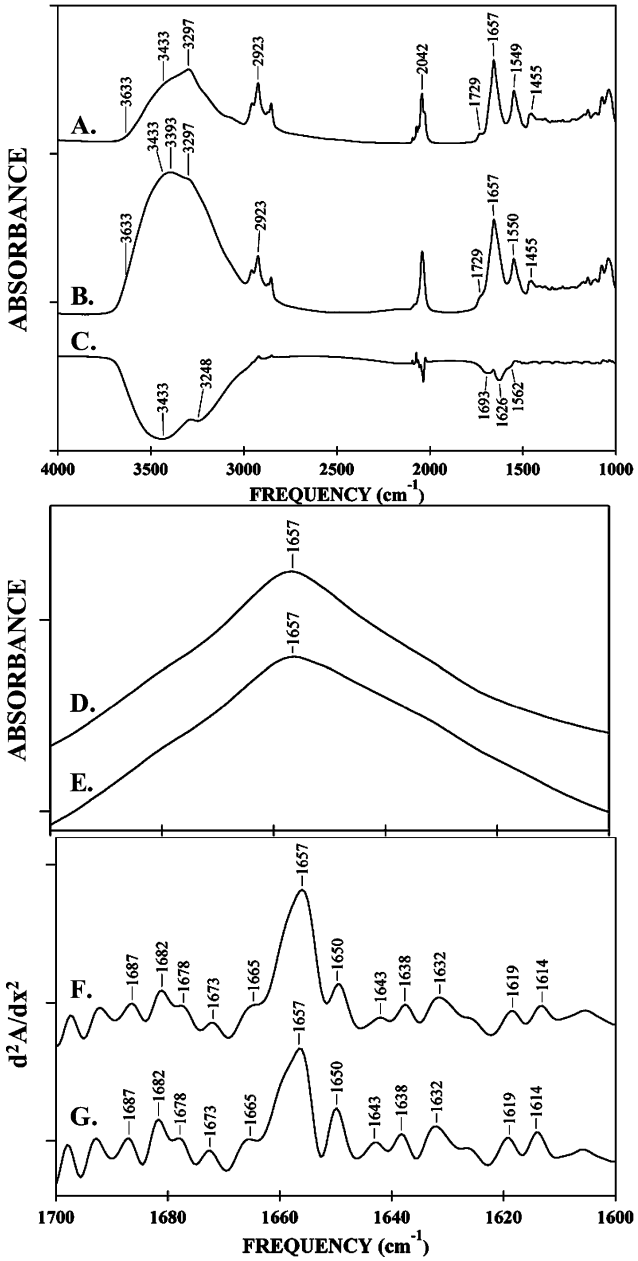

Figure 4. Infrared absorbance spectra of PSI. In (A), PSI was partially dehydrated, and in (B), PSI was hydrated. A one-to-one subtraction of (A)-minus-(B) is shown in (C). The amide I line shapes for the dehydrated and hydrated samples are presented in (D) and (E), respectively. Inflection points in the amide I line shape, which are often assigned to specific secondary structural elements, are presented as the second derivative [dehydrated (F) and hydrated (G)]. Tick marks on the *y*-axis represent 1 absorbance unit for spectra A, B, and C and 0.5 absorbance units for D and E. Conditions and procedures are given in the Materials and Methods section.

that $P_{700}^+/F_{A/B}^-$ charge recombination makes only a small contribution to the observed P_{700}^+ decay kinetics at 263 K. Therefore, we attribute the observed rate at 263 K to P_{700}^+ reduction by bound potassium ferrocyanide.

Hydration Effects on the PSI FT-IR Spectrum. The infrared absorbance spectra of partially dehydrated and hydrated PSI samples are shown in Figure 4A and B, respectively. These spectra have been normalized for protein content using the amide II band at 1549 cm^{-1}. The broad peaks observed in Figure 4

(30) Warden, J. T., Jr.; Mohanty, P.; Bolton, J. R. *Biochem. Biophys. Res. Commun.* **1974**, *59*, 872−878.

include OH/NH stretching modes from 3700 to 3300 cm^{-1}, CH stretching modes at 2900 cm^{-1}, C≡N stretching modes at 2042 cm^{-1}, and amide I, II, and III bands between 1700 and 1200 cm^{-1}.[31] Pure water has vibrational modes in the OH stretching and HOH bending regions. The broad OH stretching band falls between 3633 and 3260 cm^{-1}.[32,33] The OH bending vibration has been shown to contribute to the spectrum between 1703 and 1610 cm^{-1}.[33] As shown in Figure 4, water makes a less significant contribution in dehydrated PSI (Figure 4A) and makes a substantially increased contribution to the broad OH band in the hydrated sample (Figure 4B). The difference (Figure 4A,B) is shown in Figure 4C. This difference spectrum is dominated by water vibrational modes, caused by the decrease in water content in Figure 4A, compared to that in Figure 4B. In the 1800−1200 cm^{-1} region, the observed water bands are broad negative bands, with maxima at 1693(−) and 1626(−) cm^{-1}.

The relative intensity of the infrared bands in the OH stretching region (3400 cm^{-1}) and the amide II region (1550 cm^{-1}) can be ratioed to give an estimate of water content.[34] Using a correlation previously published for another photosynthetic reaction center,[35] we would estimate the relative humidity of the hydrated sample as ∼100% (Figure 4B) and the dehydrated sample as ∼60% (Figure 4A).

With dehydration, removal of water would be expected to occur first at the surface of the protein. Removal of surface water could lead to changes in secondary structure or to intermolecular aggregation. These structural changes may, in turn, lead to alterations in hydrogen bonding, which can be detected as changes to the amide I line shape.[36] In secondary structure analysis, the amide I line shape is viewed as the superposition of amide I bands, differing in frequency and arising from different secondary structural elements in the protein.[37] As shown in Figure 4D and E, no dramatic changes in amide line shape were observed when the dehydrated (Figure 4D) and hydrated (Figure 4E) samples were compared. To reveal more subtle changes, second derivative analysis was performed (Figure 4F and G). Second derivative analysis reveals inflection points in the amide I band, which can be assigned to α-helical, *β*-strand, random coil turns, and intermolecular hydrogen bonding in proteins (for examples, see refs 38−40 and references therein). As shown in Figure 4F, dehydration of the sample caused no significant change in the results of second derivative analysis (compare Figure 4F to G). These data provide evidence that dehydration does not cause changes in the ground state secondary structure of PSI.

Hydration Effects on the FT-IR Difference Spectrum Associated with P_{700} Oxidation. In Figure 5, light-minus-dark FT-IR spectra, associated with P_{700}^+-minus-P_{700}, are presented in the 4000−1000 cm^{-1} region. Figure 5A,C shows the light-minus-dark difference spectra obtained under continuous illumination for partially dehydrated (Figure 5A) and hydrated (Figure 5C) PSI. The hydration levels are described by the ground state data in Figure 4A and B, respectively. The bands observed in the 1800−1200 cm^{-1} region of Figure 5A and C are similar to each other and to spectra previously reported.[14,18,41] Except for changes in the CN stretching vibrations of potassium ferricyanide and ferrocyanide at ∼2100 cm^{-1},[42] dehydration has no dramatic effect on the light-minus-dark spectrum. The observed spectral features are significant when compared to two different measurements of the spectral noise (Figure 5E and F). Figure 5E is a dark-minus-dark control. An additional control (Figure 5F) was obtained by subtracting one-half of a light-minus-dark data set from the other half of that same data set and dividing by the square root of two. This control spectrum is not expected to exhibit vibrational bands and is another measure of the noise in the experiment.

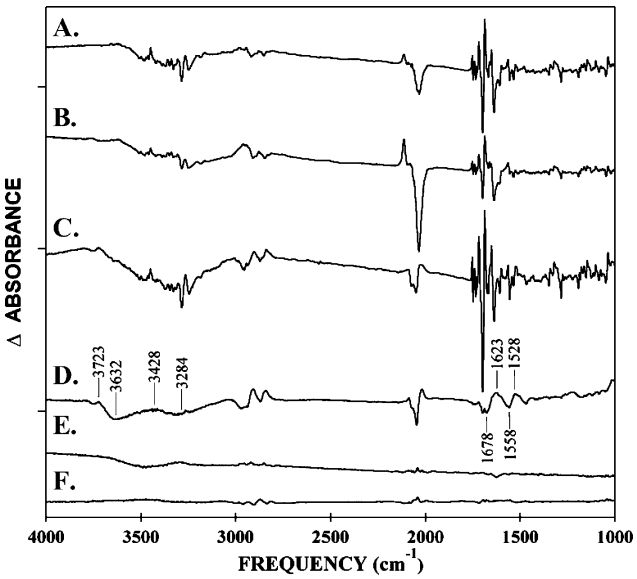

Figure 5. Hydration effects on the 4000−1000 cm^{-1} region of the light-minus-dark FT-IR difference spectrum. The difference spectra correspond to P_{700}^+-minus-P_{700}. In (A) and (C), difference spectra were acquired under illumination from partially dehydrated and hydrated PSI, respectively. In (B) and (D), difference spectra were obtained immediately after illumination from partially dehydrated and hydrated PSI, respectively. A dark-minus-dark control is presented in (E). In (F), a one-to-one control subtraction is shown, which should contain no vibrational bands. To generate this control, the individual spectra averaged to give (A) were divided into two data sets. In (F), these two data sets were subtracted and divided by $\sqrt{2}$ to compare to (A−D). Tick marks on the *y*-axis represent $\Delta 2 \times 10^{-3}$ absorbance units. Spectral conditions are given in the Materials and Methods section.

Figure 5B,D presents P_{700}^+-minus-P_{700} spectra obtained immediately after illumination in the dehydrated and hydrated samples. These data give an estimate of the amount of P_{700}^+ relaxation that occurs over 4 min in the dark. The partially dehydrated spectrum provides evidence of a slower decay (Figure 5B), in that narrow bands associated with the P_{700}^+-minus-P_{700} spectrum still remain after illumination has ceased. By contrast, the hydrated sample (Figure 5D) shows only broad features that can be associated with vibrational bands of water, detergent, ferri/ferrocyanide, and the peptide bond. In particular, the spectrum in Figure 5D exhibits no significant contribution

(31) Krimm, S.; Banderkar, J. *Adv. Protein Chem.* **1986**, *38*, 181−364.
(32) Fischer, W. B.; Eysel, H. H. *J. Mol. Struct.* **1997**, *415*, 249−257.
(33) Fischer, W. B.; Fedorowicz, A.; Koll, A. *Phys. Chem. Chem. Phys.* **2001**, *3*, 4228−4234.
(34) Patzlaff, J. S.; Moeller, J. A.; Barry, B. A.; Brooker, R. J. *Biochemistry* **1998**, *37*, 15363−15375.
(35) Noguchi, T.; Sugiura, M. *Biochemistry* **2002**, *41*, 2322−2330.
(36) Jackson, M.; Mantsch, H. H. *Crit. Rev. Biochem. Mol. Biol.* **1995**, *30*, 95−120.
(37) Surewicz, W. K.; Mantsch, H. A.; Chapman, D. *Biochemistry* **1993**, *32*, 389−394.
(38) Dong, A.; Huang, P.; Caughey, W. S. *Biochemistry* **1990**, *29*, 3303−3308.
(39) Torii, H.; Tasumi, M. *J. Chem. Phys.* **1992**, *96*, 3379−3387.
(40) Pelton, J. T.; McLean, L. R. *Anal. Biochem.* **2000**, *277*, 167−176.
(41) Hastings, G.; Ramesh, M.; Wang, R.; Sivakumar, V.; Webber, A. *Biochemistry* **2001**, *40*, 12943−12949.
(42) Kim, S.; Barry, B. A. *Biophys. J.* **1998**, *74*, 2588−2600.

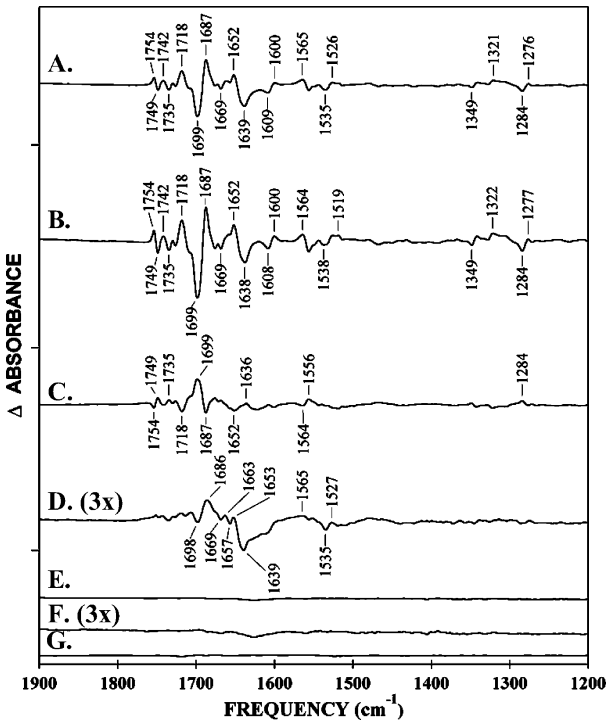

Figure 6. Hydration effects on the 1900−1200 cm^{-1} region of the light-minus-dark FT-IR difference spectrum. The P_{700}^+-minus-P_{700} spectra, acquired either from partially dehydrated or from hydrated PSI, is shown in (A) and (B), respectively. The double difference spectrum (C) was obtained using a one-to-one subtraction of partially dehydrated (A)-minus-hydrated (B) data. In (D), an interactive subtraction of partially dehydrated-minus-hydrated was performed to minimize spectral contributions between 1760 and 1720 cm^{-1}. The resulting spectrum was multiplied by a factor of 3. A dark-minus-dark control is presented in (E). In (F), the dark-minus-dark control was multiplied by a factor of 3. In (G), a one-to-one control subtraction is shown, which should contain no vibrational bands. To generate this control, the spectra averaged to give (A) were divided into two data sets. In (G), these two data sets were subtracted and divided by $\sqrt{2}$ to compare to (A−D). Tick marks on the *y*-axis represent $\Delta 5 \times 10^{-3}$ absorbance units. Spectral conditions are given in the Materials and Methods section.

from chl oxidation bands. This FT-IR-detected slowing of the P_{700}^+ decay rate is in agreement with the results of our EPR measurements on partially dehydrated samples (Figure 3).

Figure 5D suggests that there are slow water, detergent, and protein relaxation events, which follow P_{700}^+ decay in hydrated PSI. For example, CH stretching modes, most likely associated with the detergent in the PSI micelle, can be observed at 2900 cm^{-1}. The broad nature of these bands and the fact that a broad water band is also observed at 3632 cm^{-1} suggest that detergent−protein and water−protein interactions are altered as PSI relaxes into the ground state. The bands at 3428 and 3284 cm^{-1} are assignable either to hydrogen-bonded water molecules or to the NH stretching vibration of the protein backbone. Bands at 1558 and 1528 cm^{-1} may be assignable to the amide II vibration of the peptide bond; bands at 1678 and 1623 cm^{-1} may be assignable to the amide I vibration.[31] There may also be broad contributions from OH bending modes of water. The idea that protein relaxation accompanies electron transfer in PSI has been suggested previously.[15]

The 1900−1200 cm^{-1} region of the light-minus-dark spectra in Figure 5A and C are shown in Figure 6A and B. Vibrational modes associated with chl *a* oxidation are expected in this spectral region. On the basis of isotopic labeling of chl, the bands at 1754(+)/1749(−) and 1742(+)/1735(−) cm^{-1} have been assigned to chl *a* 13^3 ester, C═O vibrations.[43] It has been proposed that a differential feature at 1699(−)/1718(+) cm^{-1} may be assigned to an upshift of the 13^1 keto, C═O vibration with chl oxidation.[44] The assignment of other bands has been controversial[14,18,19,45] and will be discussed below.

In Figure 6, the P_{700}^+-minus-P_{700} spectrum was obtained either in partially dehydrated (Figure 6A) or in hydrated (Figure 6B) samples. These spectra have been corrected for any small difference in protein concentration and path length using the amide II band at ∼1550 cm^{-1}.[14] The light-minus-dark difference spectrum in the hydrated sample (Figure 6B) is approximately 1.6 times larger in amplitude compared to the spectrum in the partially dehydrated sample (Figure 6A). Because the spectra are corrected for any small difference in path length or protein concentration, this result suggests that the yield of oxidized P_{700} is increased in the wet samples relative to the partially dehydrated.

Figure 6C shows a double difference spectrum, which is the result of subtracting Figure 6B (hydrated) from Figure 6A (partially dehydrated) on a one-to-one basis. The spectrum reflects the difference in the yield of P_{700} oxidation, as well as dehydration effects on the spectrum. If these spectra are instead interactively subtracted to minimize the ester carbonyl bands at 1754(+)/1749(−) cm^{-1} (Figure 6D), small band shifts associated with the change in hydration are observed. This procedure reveals frequency differences caused by dehydration of the sample. The peaks observed in Figure 6D are above the noise as represented by the controls in Figure 6E and F. The observed spectrum is distinct from the water spectrum, observed in Figure 4C, because narrow bands are observed at 1698(−), 1686(+), 1653(+), 1639(−), 1565(+), 1535(−), and 1527(+) cm^{-1}. We favor the assignment of these bands to P_{700} and P_{700}^+. This spectrum (Figure 6D) reflects changes in the interactions of P_{700}^+ and P_{700} with bound water molecules in PSI and will be discussed below. Note that there may also be underlying, broad spectral contributions that result from removal of water in Figure 6C (see Figure 4C).

Figure 7 presents the same data, but shows the region between 3800 and 2800 cm^{-1} for partially dehydrated (Figure 7A) and hydrated (Figure 7B) samples. The amide II-corrected and carbonyl-minimized double differences are shown in Figure 7C and D, and spectral controls are shown in Figure 7E and F. The same subtraction parameters were used in Figures 6 and 7. The ester carbonyl-minimized spectrum (Figure 7D) shows differential bands in the 3800−2800 cm^{-1} region, which will be discussed below.

Deuteration of the Tyrosine Aromatic Ring Alters the P_{700}^+-minus-P_{700} Spectrum. PSI was isolated from cyanobacteria grown in the presence of $^2H_4$ ring-labeled tyrosine. This method has been previously described and results in quantitative labeling of the tyrosine ring.[20,46] There is no detectable scrambling of label from isotopically labeled tyrosine into chlorophyll or the peptide bond.[46,47] FT-IR spectroscopy was performed on the tyrosine-labeled PSI sample to evaluate the

(43) Kim, S.; Barry, B. A. *J. Am. Chem. Soc.* **2000**, *122*, 4980−4981.
(44) Nabedryk, E.; Leonhard, M.; Mäntele, W.; Breton, J. *Biochemistry* **1990**, *29*, 3242−3247.
(45) Wang, R.; Sivakumar, V.; Johnson, T. W.; Hastings, G. *Biophys. J.* **2004**, *86*, 1061−1073.
(46) Kim, S.; Patzlaff, J.; Krick, T.; Ayala, I.; Sachs, R. K.; Barry, B. A. *J. Phys. Chem. B* **2000**, *104*, 9720−9727.

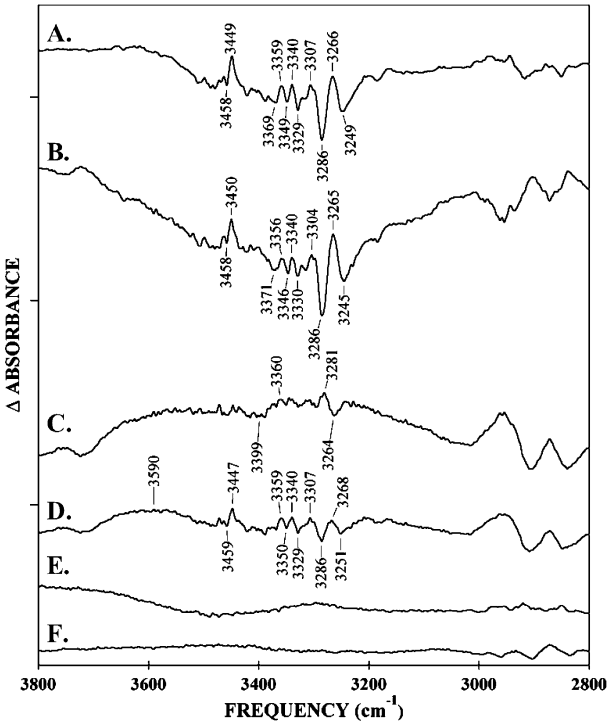

Figure 7. Hydration effects on the 3800−2800 cm^{-1} region of the light-minus-dark difference FT-IR spectra. The P_{700}^+-minus-P_{700} spectra, acquired either from partially dehydrated or from hydrated PSI, are shown in (A) and (B), respectively. The double difference spectrum (C) was obtained using a one-to-one subtraction of partially dehydrated (A)-minus-hydrated (B). In (D), an interactive subtraction of partially dehydrated-minus-hydrated was performed to minimize spectral contributions between 1760 and 1720 cm^{-1}. The subtraction parameter in (D) is the same as the value used to generate Figure 6D. A dark-minus-dark control is presented in (E). In (F), a one-to-one control subtraction is shown, which should contain no vibrational bands. To generate this control, the spectra averaged to give (A) were divided into two data sets. In (F), these two data sets were subtracted and divided by $\sqrt{2}$ to compare to (A−D). Tick marks on the *y*-axis represent $\Delta 1 \times 10^{-3}$ absorbance units. Spectral conditions are given in the Materials and Methods section.

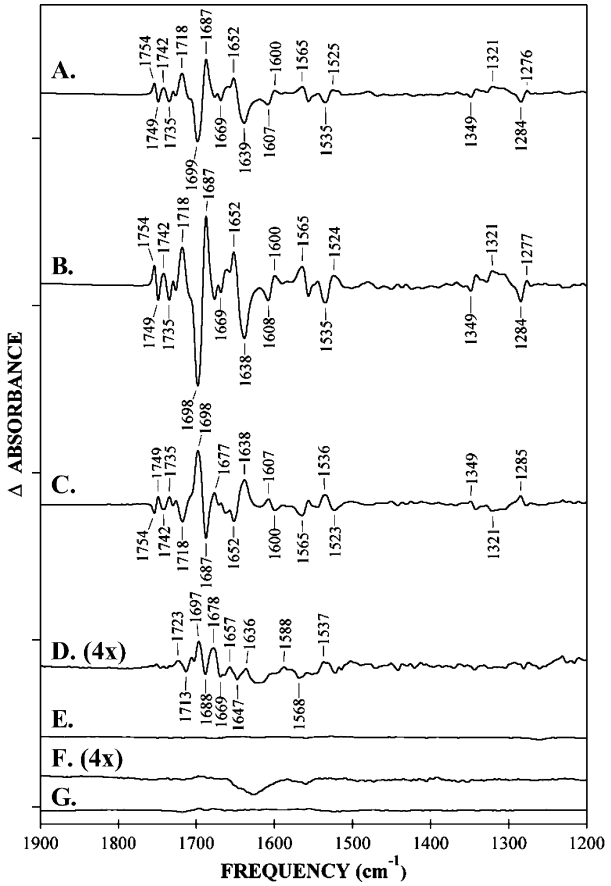

Figure 8. Effects of $^2H_4$ Tyr labeling on the 1900−1200 cm^{-1} region of the light-minus-dark FT-IR difference spectrum. The P_{700}^+-minus-P_{700} spectra, acquired either from control $^1H_4$ Tyr PSI or from labeled $^2H_4$ Tyr PSI, are shown in (A) and (B), respectively. The double difference spectrum (C) was obtained using a one-to-one subtraction of $^1H_4$ Tyr (A)-minus-$^2H_4$ Tyr (B). In (D), an interactive subtraction of $^1H_4$ Tyr-minus-$^2H_4$ Tyr was performed to minimize spectral contributions between 1760 and 1720 cm^{-1}. The resulting spectrum was multiplied by a factor of 4. A dark-minus-dark control is presented in (E). In (F), the dark-minus-dark control was multiplied by a factor of 4. In (G), a one-to-one control subtraction is shown, which should contain no vibrational bands. To generate this control, the spectra averaged to give (A) were divided into two data sets. In (G), these two data sets were subtracted and divided by $\sqrt{2}$ to compare to (A−D). Tick marks on the *y*-axis represent $\Delta 5 \times 10^{-3}$ absorbance units. These samples were partially dehydrated. Spectral conditions are given in the Materials and Methods section.

contribution of tyrosine vibrational bands to the P_{700}^+-minus-P_{700} spectrum. The 1900−1200 cm^{-1} region of the control light-minus-dark difference spectrum is shown in Figure 8A; the light-minus-dark difference spectrum for the $^2H_4$ tyrosine deuterated sample is shown in Figure 8B. Dark and subtraction controls are presented as Figure 8E−G. Figure 9 shows the same set of spectra but in the 3600−3100 cm^{-1} region of the infrared spectrum. A difference in the magnitude of chl oxidation can be seen when the control and labeled samples are compared (compare Figure 8A and B and compare Figure 9A and B). A larger amplitude is observed in the deuterated PSI sample (Figure 8B and Figure 9B). Therefore, the one-to-one subtracted spectrum reflects mainly this difference in the yield of P_{700} (Figure 8C and Figure 9C). However, the carbonyl-minimized interactive spectrum (Figure 8D and 9D) shows isotope shifts caused by $^2H_4$ labeling of tyrosine. This result suggests that oxidation of P_{700} results in reorientation of tyrosine side chains in PSI. However, there is no difference in the relative rate of spectra decay after illumination when tyrosine is labeled (data not shown). A more detailed interpretation of these isotope shifts is given below.

Discussion

Assignments of the P_{700}^+-minus-P_{700} Spectrum. The structural changes associated with the oxidation of P_{700} can be assessed through the use of reaction-induced (light-minus-dark) FT-IR spectroscopy. Oxidation of chl in vitro upshifts the frequencies of the ester and keto group (Figure 1A) and also alters macrocycle vibrations.[44] While FT-IR measurements have been interpreted to support a symmetric spin distribution in P_{700}^+,[18,19] magnetic resonance measurements on P_{700}^+ support an asymmetric spin distribution, with 85% of the spin located on P_B.[17,48]

While it is agreed that hydrogen bonding of the P_A 13^1 keto (Figure 1A) carbonyl[3] will lower the keto vibrational frequency of P_A, relative to P_B, the question of FT-IR band assignments for P_{700} has not been resolved. An isotopic labeling experiment

(47) Pujols-Ayala, I.; Sacksteder, C. A.; Barry, B. A. *J. Am. Chem. Soc.* **2003**, *125*, 7536−7538.

(48) Petrenko, A.; Maniero, A.; van Tol, J.; MacMillan, F.; Li, Y.; Brunel, L.; Redding, K. *Biochemistry* **2004**, *43*, 1781−1786.

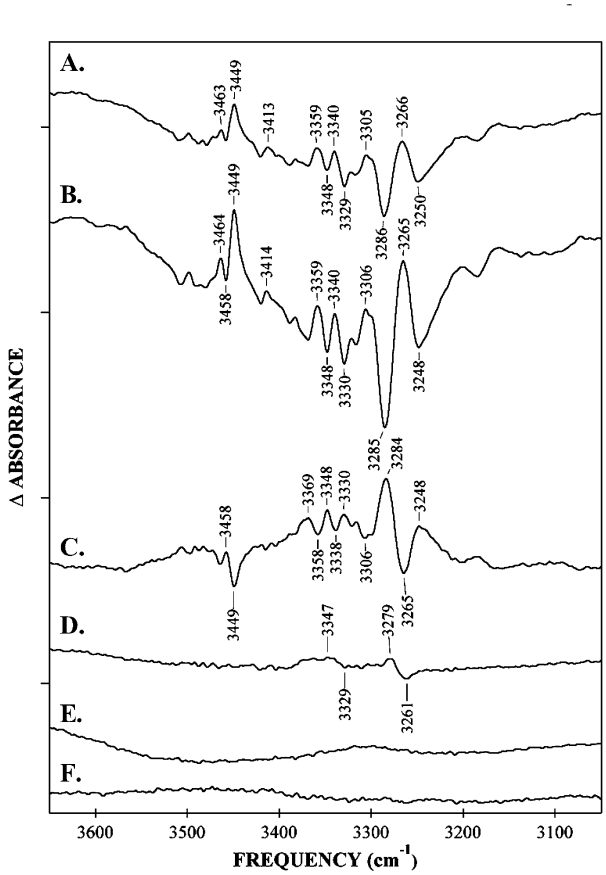

Figure 9. Effects of $^2H_4$ Tyr labeling on the 3650−3050 cm^{-1} region of the light-minus-dark FT-IR difference spectrum. The P_{700}^+-minus-P_{700} spectra, acquired either from control $^1H_4$ Tyr PSI or from labeled $^2H_4$ Tyr PSI, are shown in (A) and (B), respectively. The double difference spectrum (C) was obtained using a one-to-one subtraction of $^1H_4$ Tyr (A)-minus-$^2H_4$ Tyr (B). In (D), an interactive subtraction of $^1H_4$ Tyr-minus-$^2H_4$ Tyr was performed to minimize spectral contributions between 1760 and 1720 cm^{-1}. The subtraction parameter in (D) is the same as the value used to generate Figure 8D. A dark-minus-dark control is presented in (E). In (F), a one-to-one control subtraction is shown, which should contain no vibrational bands. To generate this control, the spectra averaged to give (A) were divided into two data sets. In (F), these two data sets were subtracted and divided by $\sqrt{2}$ to compare to (A−D). Tick marks on the *y*-axis represent $\Delta 0.5 \times 10^{-3}$ absorbance units. These samples were partially dehydrated. Spectral conditions are given in the Materials and Methods section.

has been used to assign bands to the ester group of P_A and P_B.[43] In this experiment, the methyl group of the chl ester moiety was specifically deuterated by labeling of methionine. This approach identified four differential bands that were sensitive to methyl group deuteration at 1754(+)/1750(−), 1745(+)/1737(−), 1730(+)/1726(−), and 1720(+)/1714(−) cm^{-1}. The isotope shift of each differential feature was concluded to be small, resulting in equal intensity in each of four differential features. These equal isotope-shifted intensities argue against interpretations in which only two ester C═O vibrations, one from P_A and one from P_B, contribute to the spectrum.[18,45] The observation of more C═O frequencies than predicted by the P_A/P_B dimer structure was explained by the idea that some chemical process, such as partial enolization, lead to a heterogeneity in structure and distribution of frequencies for P_A, P_B, or both.[43] ^2H solvent exchange, at pH 7.5, also supported the idea of a distribution of frequencies for the ester C═O stretching vibration.[14] These experiments were performed on frozen samples at −10 °C, where solvent viscosity is not expected to influence the results.

Three sets of P_{700} keto C═O assignments have been proposed. Breton et al. suggest that hydrogen bonding causes a downshift of both ground-state and oxidized keto C═O bands of P_A and P_B. In this interpretation, the 1718(+)/1699(−) cm^{-1} bands are assigned to chl *a* (P_B) and the 1652(+)/1639(−) bands are assigned to chl *a*′ (P_A).[18,49] The large downshift of the keto vibration of P_A was attributed to a strong hydrogen bond with the keto oxygen. Hastings et al. propose that the keto C═O bands of both P_A and P_B contribute at ∼1699(−) cm^{-1}. Upon photooxidation of P_{700}, the keto C═O band of P_B upshifts to 1718 cm^{-1} and the keto C═O band of P_A downshifts to 1687 cm^{-1}.[41,45] This explanation is in synchrony with the observation that the unpaired spin is localized on P_B, and not on P_A.[17,48] Kim et al. have proposed that multiple bands in the keto carbonyl region, when PSI samples are ^2H exchanged, are distributed due to partial enolization of P_A and/or P_B.[14] Enolization could explain the low midpoint potential of P_{700}, compared to chl *a* in organic solvents,[16] and might be consistent with a structural distortion reported in the chlorin ring of the PSI primary donor.[3]

Dehydration Effects on the Structure of P_{700} as Assessed by FT-IR Spectroscopy. Overall, we report here that the effect of dehydration on the light-minus-dark spectrum is not dramatic. Removal of water has only a small effect on most of the bands in the 3500, 2500, and 1800−1200 cm^{-1} regions. For example, a differential band from the cysteine S−H is observed at 2500 cm^{-1} under both sets of conditions (data not shown). However, we do observe interesting small effects on the spectrum, which we attribute to water removal and an alteration in the interaction of P_A with its hydrogen-bonding network (Figure 1B).[2,3,5] Note that we are not proposing that our dehydration procedure specifically removes the water molecules observed in the crystal structure. Rather, our data suggest that additional internal water molecules may play a role in PSI structure and function.

One possible interpretation of the double difference spectrum, associated with P_{700} dehydration, is that a band at 1639 cm^{-1}, originating from the ground state of P_A (chl *a*′) shifts up to 1653 cm^{-1} when P_A is oxidized, and that both of these bands upshift upon hydration. That is, hydration causes a shift of the 1639(−) cm^{-1} band of P_A to 1686 cm^{-1} and the 1653(+) cm^{-1} band of P_A^+ to 1698 cm^{-1}. This interpretation is based on the idea that removal of water increases the strength of a hydrogen bond between a threonine[5] and P_A, and thus causes a decrease in frequency for the keto C═O bands. This explanation is based on previous work, in which an upshift was observed for 1638(−) and 1658(+) cm^{-1} bands, assigned to P_A, when site-directed mutations were generated at threonine A379.[5] The 1638 cm^{-1} band shifted to 1657, 1669, and 1672 cm^{-1} in the TY, TH, and TV mutants, respectively. The 1658 cm^{-1} band shifted to 1688 cm^{-1} in every mutant. The upshift in P_A bands was attributed to loss of a hydrogen bond from the threonine to the P_A keto group. Similar observations have been reported by others.[19,50]

The frequencies of the 1639 and 1653 cm^{-1} bands in our spectra are similar to frequencies assigned in ref 5 to P_A. Also, our hydration results are in agreement with the direction of the

(49) Breton, J. *Biochim. Biophys. Acta* **2001**, *1307*, 180−193.
(50) Wang, R.; Sivakumar, V.; Li, Y.; Redding, K.; Hastings, G. *Biochemistry* **2003**, *42*, 9889−9897.

shift observed in these threonine mutants, except that the magnitude of the upshift is larger (+10 cm^{-1}) in our data. The larger magnitude of the shift in our data could be caused by the removal of additional water molecules near P_A in our experiment. In this interpretation of our data, threonine makes a stronger hydrogen bond to the keto oxygen when nearby water molecules are removed. The increase in hydrogen bonding strength could be caused by the decreased polarity of the P_A environment.

Another possible interpretation of the double difference spectrum is that the removal of water alters the extent of tautomerization of P_A. In this explanation, the upshift that we observe in the spectrum when the sample is hydrated is due to an increase in double bond character and a decrease in the extent of enolization when P_{700} is hydrated.[14] Such a low frequency (1639 cm^{-1}) in P_A for a keto vibration is consistent with a change in double bond character and tautomerization. This interpretation is supported by the fact that we observe small shoulders on the 1639/1653 cm^{-1} bands in our double difference spectra, which might be consistent with a distribution of spectral frequencies in P_A.

The amplitude of the dehydration-induced double difference spectrum is small compared to that of the difference spectrum. Analysis of the amplitude suggests that water has not been removed in all PSI reaction centers. However, using this dehydration procedure, we do see a large effect on the rate of P_{700}^+ reduction (see discussion below), suggesting that the amount of water removed is significant and that water has a functional role in PSI.

In another proposal,[41,45] the 1658 and 1638 cm^{-1} bands are assigned to ligating histidine vibrations. Bands at 1699(−) and 1687(+) cm^{-1} are assigned to P_A and P_A^+, respectively. The samples employed in these studies were hydrated samples.[41,45] It is difficult to rationalize why removal of water should alter ligand vibrational bands. However, the question of assignment of the keto bands of P_{700} awaits definitive resolution by chl labeling.

In the 1800−1200 cm^{-1} region, we also observe broad spectral features at 1565(+), 1535(−), and 1527(+) cm^{-1}, which we attribute to dehydration-induced frequency changes in P_A macrocycle vibrations. The frequencies of chl macrocycle bands are known from previous Raman studies.[51] In this previous work,[51] bands at 1560 and 1530 cm^{-1} were assigned to CC stretching vibrations of the chl *a* macrocycle. The macrocycle vibrational spectrum is expected to respond to change in double bond character at the keto oxygen because this reaction changes the planarity of the chlorin ring.

Dehydration also causes small changes in the 3800−2800 cm^{-1} region of the spectrum. The double difference spectrum shows five derivative-shaped bands between 3460 and 3250 cm^{-1}. We attribute these bands in our double difference spectrum to dehydration-induced changes in OH/NH stretching vibrations in the vicinity of P_{700}.[14] Because there are tyrosine and threonine side chains in the vicinity (Figure 1B) of both P_A and P_B, a possible assignment of these bands is to threonine and tyrosine OH stretching vibrations.

One conclusion to be drawn from our data is that the extent of hydration has the potential to alter the vibrational frequencies of P_{700}/P_{700}^+. This may be a source of uncertainty in comparing FT-IR spectra from different groups. To reduce background contributions from water, FT-IR samples are often extremely concentrated or partially dehydrated. The extent of hydration is an important variable that needs to be considered in comparing FT-IR assignments for PSI. It is possible that variation in the hydration level of individual PSI reaction centers led to the distribution of frequencies previously noted for the ester C═O vibrations of P_{700}.[43] However, the observation of a very similar, distributed pattern of isotope-shifted frequencies upon quantitative ^2H labeling of PSI (from growth of cyanobacteria in ^2H_2O media) would argue against this conclusion because those quantitatively ^2H-labeled PSI samples were hydrated.[45]

Kinetic Effects Associated with Dehydration at −10 °C. When PSI is dehydrated, we observe a slowing of the rate of P_{700}^+ reduction both with EPR spectroscopy and with difference FT-IR spectroscopy. On the basis of the FT-IR results described above, we interpret the cause of the kinetic effects as removal of water, which is located in the hydrogen-bonding network of P_{700}. We observe that removal of water slows the rate of P_{700}^+ reduction by ferrocyanide by 2 orders of magnitude. In room temperature experiments in solution, this might be attributed to a diffusion limitation. However, these kinetic experiments were performed on frozen samples (at −10 °C) on solid supports. This result suggests that water near the primary donor (Figure 1B) plays an important role in facilitation of electron transfer. This change could be caused by a change in reorganization energy for the media surrounding P_{700}, a polarity-induced change in P_{700} midpoint potential, or a dehydration-induced conformational change in PSI. Such a change is consistent with a role for tautomerization in P_{700} redox reactions because restriction in the amount of available water may slow the rate of enolization. Such a change is also consistent with a redox-induced change in hydrogen bond strength because the electron-transfer rate may be limited by a shift in hydrogen bond distance and in partial proton transfer.

Viscosity Effects on P_{700}^+ Reduction at Room Temperature. We report here that the reduction of P_{700}^+ shows a viscosity effect at pH 7.5 and 8.0, but not at pH 7.0. Viscosity changes alter dynamics in proteins, such as myoglobin, ribonuclease, and the photosynthetic reaction center.[52−56] It has also been reported that protein reorganization may be of importance to the PSI electron-transfer process.[15] Together with our result, this conclusion would suggest that the effect of viscosity on P_{700}^+ reduction reflects an inhibition of PSI protein dynamics. Additional support for the role of protein dynamics is the decreased kinetics in glycerol, relative to that of sucrose or ^2H_2O. It has been suggested that the hydroxylic nature of viscosogens, such as glycerol, can cause protein structural effects that interfere with reaction kinetics.[57,58] Note that decreased rates of P_{700}^+ reduction were not observed in glycerol or ^2H_2O at p^1H/p^2H

(51) Boldt, N. J.; Donohoe, R. J.; Birge, R. R.; Bocian, D. F. *J. Am. Chem. Soc.* **1987**, *109*, 2284−2298.
(52) Oh-oka, H.; Iwaki, M.; Itoh, S. *Biochemistry* **1997**, *36*, 9267−9272.
(53) Keefe, S. E.; Grant, E. H. *Phys. Med. Biol.* **1974**, *19*, 701−707.
(54) Ansari, A.; Jones, C. M.; Henry, E. R.; J. H.; Eaton, W. A. *Biochemistry* **1994**, *33*, 5128−5145.
(55) Beece, D.; Eisenstein, L.; Frauenfelder, H.; Good, D.; Marden, M. C.; Reinisch, L.; Reynolds, A. H.; Sorensen, L. B.; Yue, K. T. *Biochemistry* **1980**, *19*, 5147−5157.
(56) Rector, K. D.; Jiang, J.; Berg, M. A.; Fayer, M. D. *J. Phys. Chem. B* **2001**, *105*, 1081−1092.
(57) Palazzo, G.; Mallardi, A.; Hochkoeppler, A.; Cordone, L.; Venturoli, G. *Biophys. J.* **2002**, *82*, 558−568.
(58) Roth, J. P.; Klinman, J. P. *Proc. Natl. Acad. Sci. U.S.A.* **2002**, *100*, 62−67.

7.0. These observations support the conclusion that proton transfer is important in the P_{700}^+ reduction process. Our data suggest that this proton transfer is not rate limiting at low pH, but that the inhibition of protein dynamics at increased viscosity shifts the rate-limiting step to one requiring protons. This putative proton transfer reaction may be directly linked to electron transfer, in a process such as redox-linked changes in chl enolization or chl hydrogen bonding. However, it could also reflect a long-range structural interaction, involving an amino acid such as histidine. A pH-dependent viscosity effect has previously been observed in rates of electron transfer to dioxygen in glucose oxidase.[59] It was later determined that this was due to a shift in the pK_a of a histidine; the protonation of this residue was found to be important to the electron-transfer process.[58] In our previous work, we suggested that a long-range structural change may accompany the oxidation and reduction of P_{700} at pH 7.5.[14] The pH-dependent viscosity effects reported here support that interpretation.

Effects of Tyrosine Labeling on the P_{700}^+-minus-P_{700} Spectrum. We report here that isotopic labeling of the tyrosine aromatic side chain alters the P_{700}^+-minus-P_{700} spectrum. Because there is no detectable scrambling of label into chl or the peptide bond and little detectable scrambling into other amino acid side chains,[46,47] we conclude that structural changes in tyrosine side chains must accompany the reduction of P_{700}^+. To explain our results, we propose that P_{700}^+ reduction alters CH$-\pi$ interactions among tyrosine side chains in PSI (Figure 1B).

Tyrosines, as well as other aromatic amino acids, are known to be involved in $\pi-\pi$, $\pi-$cation, and CH$-\pi$ interactions, which stabilize proteins.[60−63] An example is an interaction between a C−H bond of the tyrosine ring and the more electronegative π-cloud of an interacting aromatic amino acid, which may also be tyrosine (Figure 1B). The physical description of this interaction is complex.[64−66] In its high energy limit, this interaction is believed to be electrostatic in nature and to resemble a weak hydrogen bond. However, in its weak energy limit, a CH$-\pi$ interaction is believed to resemble a dispersive (van der Waals) interaction. Because of this complexity, the effect of a CH$-\pi$ interaction on the vibrational spectrum of the interacting pair is not readily predictable (see refs 64−66 and references therein). The CH and aromatic ring vibrational frequencies will be altered by the interaction, but the direction and magnitude of the vibrational shifts depend on the identity of the interacting species and the geometry and energy of the interaction. Oxidation and reduction of P_{700} has been concluded to cause long-range structural changes in PSI.[14,15] Such long-range structural changes could result in alterations in CH$-\pi$ interaction distances and thus alter the frequencies of tyrosine side chains. In the immediate vicinity of the primary donor, analysis of the PSI structure[3] suggests that Y735 and Y603 in the PsaA subunit can form a CH$-\pi$ interaction (Figure 1B).

Tyrosine is expected to be in the protonated form at pH 7.5. FT-IR absorbance spectra for $^1H_4$ Tyr and $^2H_4$ Tyr have been published[67,68] and assignments have been made. Bands at 1615, 1599, and 1518 cm^{-1} have been assigned to υ_{8a}, υ_{8b}, and υ_{19} vibrational modes, respectively. In $^2H_4$ Tyr, υ_{8a} and υ_{8b} shifted to 1589 and 1577 cm^{-1}, while the υ_{19} band split into two weaker bands at 1442 and 1416 cm^{-1}. A band is observed at 1249 cm^{-1}, which is a combination of the $\upsilon_{7'a}$(CO) and δ(COH) vibrations. This band downshifts to 1225 cm^{-1} upon $^2H_4$ labeling of the tyrosine ring. The amplitude of the CO stretching vibration depends on the type and strength of hydrogen bonding to the phenol oxygen.[69]

To appear in the isotope-edited (or double difference) spectrum, vibrational frequencies must be perturbed by P_{700}^+ reduction *and* also by isotopic labeling. The isotope-sensitive frequencies that we observe in the isotope-edited spectrum are a set of second derivative-shaped bands with frequencies at 1697(+)/1688(−)/1678(+) cm^{-1} and 1657(+)/1647(−)/1636(+) cm^{-1}. Broader bands may also be observed at 1588(+), 1568(−), and 1537(+) cm^{-1}. We assign the bands at 1697(+)/1688(−)/1678(+) cm^{-1} and 1657(+)/1647(−)/1636(+) cm^{-1} to isotope-shifted υ8a and υ8b ring stretching vibrations. A second derivative-shaped band will be observed in the double difference spectrum if isotopic labeling induces a downshift of a derivative-shaped feature in the difference spectrum. The magnitude of the isotope shift cannot be deduced quantitatively from the double difference spectrum, but must be smaller than the total width of the second derivative feature. Isotope shifts of ∼20 cm^{-1} are expected from the model compound data discussed above,[67,68] and this expectation is in general agreement with the double difference spectrum. Because chl has an intense infrared spectrum, the amplitude of the tyrosine isotope-shifted spectrum is small by comparison.[44] However, the isotope-sensitive bands described here are above the noise in these measurements. Bands between 1558 and 1537 cm^{-1} may originate from υ19a of the PSI-labeled tyrosine.[67,68]

In the 3600−3100 cm^{-1} region, we observe two derivative-shaped bands in the tyrosine isotope-edited spectrum. These bands at 3279(+)/3261(−) cm^{-1} and 3347(+)/3329(−) cm^{-1} band could arise from the OH vibrations of the interacting tyrosines, which have a small isotope shift. Two sets of bands may be observed because the two interacting tyrosines are in different hydrogen-bonding environments. This could be consistent with an assignment of the interacting tyrosines to Y735 and Y603 in the PsaA subunit (Figure 1B).

Note that the putative OH stretching vibrations (∼3300−3200 cm^{-1}) are low in frequency, and the putative CC ring stretching vibrations (1690−1640 cm^{-1}) are high in frequency compared to tyrosine in aqueous solution.[67,68] This may be due to a combination of strong hydrogen-bonding interactions and the generally hydrophobic environment of the tyrosines (Figure 1B). Another factor to consider is that the electric field generated with P_{700} is oxidized. This electric field has the potential to downshift the OH stretching vibrations through a Stark effect.[70]

(59) Su, Q.; Klinman, J. P. *Biochemistry* **1999**, *38*, 8572−8581.
(60) Burley, S. K.; Petsko, G. A. *Science* **1985**, *229*, 23−28.
(61) Wang, Y.; Mao, L.; Hu, X. *Biophys. J.* **2004**, *86*, 3097−3111.
(62) Tatko, C. D.; Waters, M. L. *J. Am. Chem. Soc.* **2004**, *126*, 2028−2034.
(63) Meurisse, R.; Brasseur, R.; Thomas, A. *Proteins: Struct., Funct., Bioinformatics* **2004**, *54*, 478−490.
(64) Fujii, A.; Morita, S.-I.; Miyazaki, M.; Ebata, T.; Mikami, N. *J. Phys. Chem. A* **2004**, *108*, 2652−2658.
(65) Hermansson, K. *J. Phys. Chem. A* **2002**, *106*, 4695−4702.
(66) Hobza, P.; Havlas, Z. *Chem. Rev.* **2000**, *100*, 4253−4264.
(67) Hellwig, P.; Pfitzner, U.; Behr, J.; Rost, B.; Pesavento, R. P.; van der Donk, W.; Gennis, R. B.; Michel, H.; Ludwig, B.; Mäntele, W. *Biochemistry* **2002**, *41*, 9116−9125.
(68) Ayala, I.; Range, K.; York, D.; Barry, B. A. *J. Am. Chem. Soc.* **2002**, *124*, 5496−5505.
(69) Takeuchi, H.; Watanabe, N.; Satoh, Y.; Harada, I. *J. Raman Spectrosc.* **1989**, *20*, 233−237.
(70) Suydam, I. T.; Boxer, S. G. *Biochemistry* **2003**, *42*, 12050−12055.

Also note that there is little intensity in the 1400−1200 cm^{-1} region of the isotope-edited spectrum. This may be due to low intrinsic infrared intensity in the C−OH vibrations of the interacting tyrosines, which occurs when tyrosine is protonated and involved in a hydrogen bond as a proton acceptor.[69]

Deuteration of tyrosine did not alter the rate of reduction of P_{700}^+, as assessed from the FT-IR spectra. Therefore, we conclude that conformational changes in CH−π interactions are not rate limiting for the electron-transfer reactions. However, if changes in the energy of these interactions are thermodynamically linked to P_{700} redox reactions, these CH−π interactions could play a role in the adjustment of midpoint potential.

Summary. Previous measurements on PSI have concluded that the effective dielectric constant in PSI is high, suggesting that the electron-transfer process is accompanied by significant reorganization of protein structure.[15] This conclusion is also consistent with previous Stark measurements on the reaction center from purple bacteria.[71] Our work suggests that the PSI reorganization process alters CH−π interactions among tyrosine side chains, and if thermodynamically coupled to the electron-transfer reactions, these interactions could play a role in the control of midpoint potential and electron-transfer rate. We also have provided evidence suggesting that hydration and viscosity influence the reduction of the PSI primary donor. These results suggest a role for bound water and proton transfer in PSI electron transfer.

Acknowledgment. This work was supported by NIH GM43273 (B.A.B). We thank Dr. Ilya Vassiliev for assistance with some of the EPR measurements and Prof. David Sherrill for helpful discussions.

JA050659A

(71) Steffen, M. A.; Lao, K.; Boxer, S. G. *Science* **1994**, *264*, 810−816.
(72) Guex, N.; Peitsch, M. *Electrophoresis* **1997**, *18*, 2714−2723.